PERGAMON

International Journal of Heat and Mass Transfer 43 (2000) 3119–3135

International Journal of HEAT and MASS TRANSFER

www.elsevier.com/locate/ijhmt

Application of the statistical narrow-band correlated-*k* method to low-resolution spectral intensity and radiative heat transfer calculations — effects of the quadrature scheme

Fengshan Liu*, Gregory J. Smallwood, Ömer L. Gülder

Combustion Research Group, Institute for Chemical Process and Environmental Technology, National Research Council, Montreal Road, Ottawa, Ont., Canada K1A 0R6

Received 2 July 1999; received in revised form 15 October 1999

Abstract

The statistical narrow-band correlated-*k* method was employed to calculate low-resolution spectral intensity along a line-of-sight, and radiative heat transfer in both, a one-dimensional parallel-plates enclosure and a three-dimensional rectangular enclosure containing CO_2–H_2O–N_2 mixtures under various conditions. Numerical calculations were conducted using six quadrature schemes: the commonly used "7-point Gauss–Lobatto" quadrature, the 4-point, 2-point, and 1-point Gauss–Legendre quadratures, and the 4-point and 5-point Gauss–Lobatto quadratures. The "7-point Gauss–Lobatto" quadrature yields very accurate results compared to the results of the statistical narrow-band model. Results of the 4-point Gauss–Legendre quadrature are only slightly less accurate than those of the "7-point Gauss–Lobatto" quadrature. The 2-point Gauss–Legendre quadrature offers acceptably good accuracy with much less computing efforts, especially for calculations of spectrally integrated quantities. Results of the 1-point Gauss–Legendre are in serious error. The overall performance of the 4-point and 5-point Gauss–Lobatto quadratures is even worse than that of the 2-point Gauss–Legendre quadrature.

Keywords: Narrow-band model; Correlated-*k* method; Gauss quadrature

1. Introduction

Accurate and efficient real-gas radiation models are highly desirable in many applications and research areas of combustion. One example is the fundamental study of various flame phenomena, especially under microgravity conditions where thermal radiation is not only inherent but also a controlling mechanism of heat loss at low flame stretch [1,2]. Real gas often implies CO_2 and H_2O present in combustion products of hydrocarbon fuels and sometimes also includes CO and unburned hydrocarbons. Practically, CO_2 and H_2O are the two most important radiating gases because they exist in high concentrations in high temperature regions. Accurate calculations of real-gas radiation

* Corresponding author. Tel.: +1-613-993-9470; fax: +1-613-957-7869.

E-mail address: fengshan.liu@nrc.ca (F. Liu).

0017-9310/00/$ - see front matter
PII: S0017-9310(99)00343-9

Nomenclature

B	SNB model parameter
f	species molar fraction or the distribution function
I_i	spectral radiation intensity at the ith quadrature point (W m^{-2} cm sr^{-1})
g	cumulative distribution function
g_i	the ith Gauss quadrature point
k	absorption coefficient (m^{-1})
k_i	absorption coefficient at the ith quadrature point (m^{-1})
$\bar{k}_\nu$	mean line-intensity to spacing ratio (cm^{-1} atm^{-1})
L	path-length (m)
p	pressure (atm)
q	net heat flux (W m^{-2})
s	position variables along a line-of-sight (m)
S	SNB model parameter
T	temperature (K)
w_i	weight parameter of the ith Gauss quadrature point
x, y, z	Cartesian coordinates (m)

Greek symbols

$\bar{\beta}_\nu$	mean line-width to spacing ratio
κ_ν	gas spectral absorption coefficient (m^{-1})
$\bar{\gamma}_\nu$	mean half-width of an absorption line (cm^{-1})
$\bar{\delta}_\nu$	equivalent line spacing (cm^{-1})
ν	wavenumber (cm^{-1})
$\Delta\nu$	wavenumber interval of a band (cm^{-1})
τ_ν	gas spectral transmissivity
ξ, η, μ	direction cosines
Σ	narrow-band integrated intensity (W m^{-2} sr^{-1})

Subscripts

b	blackbody
c	CO_2
h	H_2O
ν	spectral

definitely require the resolution of the highly spectral dependence of their radiative properties. This requirement often leads to a radiation sub-model that is too computationally intensive to be used in an overall combustion model. On the other extreme, over-simplified models such as the optically thin and the grey-gas approximations are too crude to yield quantitative results. It is believed that the disagreement found between theoretical prediction and experiment can often be attributed, at least partially, to inappropriate treatment of radiation heat loss. It is interesting to note that the simplest optically thin model is still used in sophisticated numerical calculations of flame phenomena [2,3], despite its severe limitations. While use of the optically thin model in general allows the qualitative effects of radiation loss to be studied, the results often show serious error.

The statistical narrow-band (SNB) model is frequently considered the most accurate non-grey gas radiation model in the absence of line-by-line (LBL) results. In addition, the SNB model yields low-resolution spectral intensities which are required in some other applications, such as infrared detection. However, the direct implementation of this model into the radiative transfer equation (RTE) encounters severe computational difficulties in multi-dimensions because it formulates the gas radiative property in terms of transmissivity rather than the fundamental absorption coefficient [4]. Moreover, it is incompatible with radiation scattering [5]. The SNB model requires further approximation, such as the Curtis–Godson approximation, which when applied to nonisothermal and/or inhomogeneous media can give rise to significant errors under conditions of large temperature and pressure gradients [6]. Although the correlated-k fictitious gas (CKFG) method is more accurate than the SNB model, it suffers the same difficulties as the SNB model for implementation into RTE in multidimensions [6]. While the over-simplified grey-band model developed by Liu et al. [7] yields reasonably good accuracy for non-grey gas radiation in a one-dimensional parallel-plates geometry, it produces significant errors for non-grey gas radiation in multidimensions [4,8]. A systematic evaluation study of various narrow-band models, such as SNB, CK, CKFG, and global radiative property models in CO_2–H_2O–N_2 mixtures has been recently conducted by Pierrot et al. [9] using LBL results as the reference solution. They found that results of the narrow-band models are in general in very good agreement with the LBL results.

The statistical narrow-band correlated-k (SNBCK) method represents an alternative way to implement the SNB model. The method is not new in the area of atmospherical radiative transfer, but relatively new in the community of radiative heat transfer. The method has recently been applied to 2D non-grey gas radiation transfer by Goutière et al. [8]. Using the 7-point Gauss–Lobatto quadrature given in Ref. [6], they found that the SNBCK method yields almost the same accuracy as the SNB model with significantly less com-

puting effort. Their study demonstrated that the SNBCK method is an accurate and potentially efficient narrow-band method for radiative transfer calculation as well as for low-resolution spectral intensity prediction. The SNBCK method overcomes the difficulties of the SNB model due to the fact that it extracts gas absorption coefficients from the gas transmissivity. As a result, any RTE solvers, especially the efficient and accurate discrete-ordinates method (DOM), can be used. The 7-point Gauss–Lobatto has been commonly employed in various CK and narrow-band weighted-sum-of-grey-gases methods [6,10,11]. It is worth pointing out that this popular 7-point quadrature is actually not a Lobatto quadrature but a mixed Lobatto and Radau quadrature [12]. It remains to be named the "7-point Gauss–Lobatto" quadrature in the present study due to its popularity in the literature. Use of this 7-point quadrature implies that the gas radiative properties at each non-overlapping band are represented by seven grey-gases. At an overlapping band, however, the correlated treatment based on the multiplication property of gas transmissivity requires 7×7 (49) grey gases to be considered [8,13]. Therefore, the method could be quite computationally demanding in its present form, especially for scattering problems, and more research efforts are required to improve the computational efficiency of this method. The issue of overlapping bands has recently been studied by Liu et al. [14] to speed-up the execution of the SNBCK method at overlapping bands. They developed several approximate methods to treat an overlapping band as a non-overlapping band. Using the "7-point Gauss–Lobatto" quadrature and the approximate treatments of overlapping bands for spectrally integrated quantity calculations in CO_2–H_2O mixtures, they showed that the computing time can be reduced by more than 50%, while the loss of accuracy is only about 3%.

In the present study, the quantitative effects of quadrature on the accuracy and efficiency of the SNBCK method are numerically investigated for both spectrally integrated quantities and low-solution spectral intensities along a line-of-sight under typical conditions found in combustion applications. The objective of this study is to determine if fewer quadrature points can be used in the SNBCK method with minimal loss of accuracy, in comparison with the commonly used "7-point Gauss–Lobatto" quadrature. Six Gauss quadratures were considered in the present SNBCK calculations: the "7-point Gauss–Lobatto" quadrature, the 4-point, 2-point, and 1-point Gauss–Legendre quadratures, and the 4-point and 5-point Gauss–Lobatto quadratures. Results of the SNB model were also obtained as a reference solution in the evaluation of the six quadratures.

2. The SNBCK method

The SNBCK method has been discussed in length by Lacis and Oinas [13] and Goody et al. [15]. However, to assist the discussion of the present study and for the convenience of the readers, the method is briefly outlined.

The basis of CK methods is that for any radiative quantity ϕ_ν, that is solely dependent on gas absorption coefficient (this is certainly true at a narrow-band where the blackbody function can be treated as a constant), the integration over wavenumber can be replaced by integration over the absorption coefficient

$$\bar{\phi}_{\nu=}\frac{1}{\Delta\nu}\int_{\Delta\nu}\phi(\kappa_\nu)\,\mathrm{d}\nu=\int_0^\infty f(K)\phi(k)\,\mathrm{d}k \tag{1}$$

where

$$f(k)=\frac{1}{\Delta\nu}\frac{\mathrm{d}\nu}{\mathrm{d}k} \tag{2}$$

is the normalised distribution function of the gas absorption coefficient inside $\Delta\nu$ and $f(k)\,\mathrm{d}k$ represents the fraction of wavenumber inside $\Delta\nu$, where the gas absorption coefficient lies between k and $k+\mathrm{d}k$. It is worth noting that when the integration over wavenumber is replaced by integration over the gas absorption coefficient, the spectral gas absorption coefficient κ_ν is denoted by k, since it now plays the role of an independent variable and is no longer a function of wavenumber. This is equivalent to the concept of re-ordered absorption coefficient introduced in the study of Lee et al. [16]. Application of Eq. (1) to gas transmissivity leads to

$$\bar{\tau}_\nu(L)=\int_0^\infty f(k)\exp(-kL)\,\mathrm{d}k \tag{3}$$

Determination of the distribution function $f(k)$ can be done by two ways. One is to analyse the HITRAN database as has been conducted by Tang and Brewster [17]. The other is to perform the inverse Laplace transformation of the gas transmissivity of a narrow-band model based on Eq. (3), as in the SNBCK method described by Lacis and Oinas [13].

In the SNB model, the gas transmissivity over an isothermal and homogeneous path is given as [18]

$$\bar{\tau}_\nu(L)=\exp\left[-\frac{\pi B}{2}\left(\sqrt{1+\frac{4SL}{\pi B}}-1\right)\right] \tag{4}$$

where $B=2\bar{\beta}_\nu/\pi$, $S=\bar{k}_\nu fp$, L is the path-length, f the mole fraction of the radiating gas, p the pressure, and $\bar{\beta}_\nu=2\pi\bar{\gamma}_\nu/\bar{\delta}_\nu$ the average line-width to spacing ratio. The updated SNB model parameters [11], i.e. $\bar{\gamma}_\nu$, $\bar{\delta}_\nu$, and $\bar{k}_\nu$, for CO_2 and H_2O over a wide range of tem-

peratures were used in the present calculations. The bandwidth is uniform at 25 cm^{-1} and the covered spectral range is 150–9300 cm^{-1}. H_2O absorbs and emits radiation at all the 367 narrow-bands, while CO_2 has 96 radiating bands in the following four spectral regions: 450–1200 cm^{-1} (31 bands), 1950–2450 cm^{-1} (21 bands), 3300–3800 cm^{-1} (21 bands), and 4700–5250 cm^{-1} (23 bands).

The analytical expression of $f(k)$ obtained by inverse Laplace transformation of the SNB gas transmissivity given in Eq. (4) is written as [5,13]

$$f(k) = \frac{1}{2}k^{-3/2}(BS)^{1/2}\exp\left[\frac{\pi B}{4}\left(2 - \frac{S}{k} - \frac{k}{S}\right)\right] \tag{5}$$

The cumulative function $g(k)$ is defined as

$$g(k) = \int_0^k f(k')\,\mathrm{d}k' \tag{6}$$

which is a monotonically increasing function from 0 to 1. Using Eqs. (5) and (6), the analytical expression of $g(k)$ has been derived by Lacis and Oinas [13]

$$g(k) = \frac{1}{2}\left[1 - \mathrm{erf}\left(\frac{a}{\sqrt{k}} - b\sqrt{k}\right)\right] + \frac{1}{2}\left[1 - \mathrm{erf}\left(\frac{a}{\sqrt{k}} + b\sqrt{k}\right)\right]\mathrm{e}^{\pi B} \tag{7}$$

where $a = \frac{1}{2}\sqrt{\pi BS}$, $b = \frac{1}{2}\sqrt{\pi B/S}$, and $\mathrm{erf}(x)$ is the error function given as

$$\mathrm{erf}(x) = \frac{2}{\sqrt{\pi}}\int_0^x \mathrm{e}^{-t^2}\,\mathrm{d}t \tag{8}$$

Using the cumulative function g, the narrow-band average of any radiative variable ϕ_ν, dependent solely on the gas absorption coefficient κ_ν, can be calculated as

$$\bar{\phi}_\nu = \frac{1}{\Delta\nu}\int_{\Delta\nu}\phi(\kappa_\nu)\,\mathrm{d}\nu = \int_0^1 \phi(g)\,\mathrm{d}g \tag{9}$$

Eq. (9) can be conveniently calculated using a Gauss type quadrature scheme

$$\bar{\phi}_\nu = \sum_{i=1}^{N} w_i\phi(g_i) \tag{10}$$

where N is the number of quadrature points. In the execution of the SNBCK method, the value of ϕ at the ith quadrature point g_i, $\phi(g_i)$, is actually evaluated in terms of the corresponding absorption coefficient k_i, i.e. $\phi(g_i) = \phi(k_i)$. The value of k_i at a given quadrature point g_i is found by inverse use of Eq. (7), i.e. k_i is obtained iteratively by solving Eq. (7) for a known g_i using a Newton–Raphson method. Only a few iterations are required to achieve convergence of high precision if $k_{\max}$, where $f(k)$ peaks, is used as the initial guess of k_i, as suggested by Lacis and Oinas [13].

Very good accuracy is achieved using about 10 quadrature points [13,15]. The "7-point Gauss–Lobatto" quadrature has been the most popular one perhaps based on the considerations of accuracy and computer time [6,10,11]. Table 1 lists the weight parameters w_i and the quadrature point g_i of the 7-point Gauss–Lobatto scheme as given in [6].

In addition to the "7-point Gauss–Lobatto" quadrature, the 4-point, 2-point, and 1-point Gauss–Legendre quadratures and the 4-point and 5-point Gauss–Lobatto quadratures are also employed in the calculations of the SNBCK method in order to assess the quantitative effects of quadrature on the SNBCK results, in terms of accuracy and efficiency. When using a 1-point Gauss type quadrature, the SNBCK method is equivalent to the grey-band approximation developed by Liu et al. [7]. The weight parameters and quadrature points of the three Gauss–Legendre quadratures and the two Gauss–Lobatto quadratures are given in Tables 2 and 3, respectively.

For calculations of narrow-band intensities along a line-of-sight and gas radiation heat transfer in a one-dimensional parallel-plates geometry at a non-overlap-

Table 1
The "7-point Gauss–Lobatto" quadrature scheme

i	g_i	w_i
1	0.00000	0.04500
2	0.15541	0.24500
3	0.45000	0.32000
4	0.74459	0.24500
5	0.90000	0.05611
6	0.93551	0.05125
7	0.98449	0.03764

Table 2
The 1-point, 2-point, and 4-point Gauss–Legendre quadrature schemes

i	g_i	w_i
1-point		
1	0.57735	1
2-point		
1	0.33998	0.65215
2	0.86114	0.34785
4-point		
1	0.18343	0.36268
2	0.52553	0.31371
3	0.79667	0.22238
4	0.96029	0.10123

Table 3
The 4-point and 5-point Gauss–Lobatto quadrature schemes

i	g_i	w_i
4-point		
1	0.20930	0.41246
2	0.59170	0.34112
3	0.87174	0.21070
4	1.0	0.03571
5-point		
1	0.16528	0.32754
2	0.47792	0.29204
3	0.73877	0.22489
4	0.91953	0.13331
5	1.0	0.02222

ping band, the following recursive equation is solved

$$I_{i,j+1} = I_{i,j}\exp\left[-k_{i,j+1/2}(s_{j+1}-s_j)\right] + I_{b,j+1/2}\left(1 - \exp\left[-k_{i,j+1/2}(s_{j+1}-s_j)\right]\right) \quad (11)$$

where subscripts i and j denote, respectively, the ith quadrature point and jth spatial discretisation index and s is the spatial location along the direction of radiation propagation.

For radiative transfer at a non-overlapping band in three-dimensional rectangular enclosures, the transfer equation to be solved is written as

$$\xi\frac{\partial I_i}{\partial x} + \mu\frac{\partial I_i}{\partial y} + \eta\frac{\partial I_i}{\partial z} = -k_i I_i + k_i I_b, \quad i = 1, 2, \ldots, N \quad (12)$$

The band averaged radiation intensity is calculated as

$$\bar{I} = \sum_{i=1}^{N} I_i w_i \quad (13)$$

The procedures of the SNBCK method described above are applicable only for non-overlapping bands. Some modifications are required at overlapping bands. At an overlapping band, the rigorous or the correlated treatment method discussed in Refs. [8,13,14] is followed. The correlated treatment of overlapping bands consists of two steps. First, the cumulative distribution function, Eq. (7), is solved inversely to obtain the absorption coefficients of each gas component, k_{ci} and k_{hj}. Secondly, the transmissivity contributed by each component can be calculated approximately as

$$\tau_c(L) = \sum_{i=1}^{N} w_i \exp(-k_{ci}L) \quad (14)$$

$$\tau_h(L) = \sum_{j=1}^{N} w_j \exp\left(-k_{hj}L\right) \quad (15)$$

Therefore, the transmissivity of the mixture based on the multiplication property is obtained as,

$$\tau_{mix}(L) = \left(\sum_{i=1}^{N} w_i \exp(-k_{ci}L)\right)\left(\sum_{j=1}^{N} w_j \exp\left(-k_{hj}L\right)\right) = \sum_{i=1}^{N}\sum_{j=1}^{N} w_i w_j \exp\left[-\left(k_{ci}+k_{hj}\right)L\right] \quad (16)$$

The RTE at an overlapping band therefore takes the following form

$$\xi\frac{\partial I_{ij}}{x} + \mu\frac{\partial I_{ij}}{y} + \eta\frac{\partial I_{ij}}{\partial z} = -\left(k_{ci}+k_{hj}\right)I_{ij} + \left(k_{ci}+k_{hj}\right)I_b, \quad i = 1, 2, \ldots, N; j = 1, 2, \ldots, N \quad (17)$$

The band averaged radiation intensity is then calculated as

$$\bar{I} = \sum_{i=1}^{N}\sum_{j=1}^{N} w_i w_j I_{ij} \quad (18)$$

Therefore, the RTE has to be solved $N \times N$ times at each overlapping band. It is expected that the computing time of the SNBCK method increases linearly with N at non-overlapping bands and quadratically with N at overlapping bands, for two radiating species.

Spectrally integrated quantities are calculated by adding the appropriate narrow-band quantities (wall heat fluxes and volumetric source term) over all the narrow bands.

3. Results and discussions

To investigate the quantitative effects of quadrature on the results of the SNBCK method, numerical calculations were conducted for both narrow-band integrated intensities along a line-of-sight and spectrally integrated quantities (wall heat flux and radiation source term) in CO_2–H_2O mixtures under various conditions. For all the cases studied, results of the SNB model were also obtained as a reference solution in the evaluation. The discretised RTE associated with the SNB model and its solution method have been described by Kim et al. [19] and Liu et al. [4]. All the numerical calculations were carried out on a 175 MHz SGI Octane workstation.

Table 4
Column length and gas temperature distribution in the four gas columns

Column	L (m)	T (K)
1	8	1800
2	0.2	1800
3	20	1000
4	8	Eq. (19)

3.1. Narrow-band intensities along a line-of-sight

Calculations of narrow-band integrated intensities along a line-of-sight were carried out for four gas columns having different length and temperature distribution. The left end of the column is at $x = 0$ and the right end of the column is at $x = L$. We consider the narrow-band integrated radiation intensities at $x = L$ and along the positive x-direction. For all the four columns, the gas mixture is at 1 atm and consists of 10% CO_2, 20% H_2O and 70% N_2 (species concentration is specified in mole fraction throughout this study). The left bounding wall is black and at 300 K. An 81-point uniform grid was used in all the calculations. The temperature in the first three columns is uniform but in Column 4 is non-uniform. The temperature distribution in Column 4 is specified as

$$T(x) = 400 + 2000\frac{x}{x_*} \text{ for } x < x_*,$$

$$800 + 1600\frac{L-x}{L-x_*} \text{ for } x > x_* \tag{19}$$

where $L = 8$ m and $x_* = 1.5$ m. The length and gas temperature distribution in each column are summarised in Table 4.

Before results of the calculated narrow-band intensities are presented, the definitions of error and relative error used in the evaluation are introduced. Since the SNB model results are often used as the benchmark solution in the absence of LBL results, results of the SNB model are also treated as the reference or benchmark solution in the present study. Therefore, the error and relative error of the SNBCK results are defined as $(\Lambda_{\text{SNBCK}} - \Lambda_{\text{SNB}})$ and $(\Lambda_{\text{SNBCK}} - \Lambda_{\text{SNB}})/\Lambda_{\text{SNB}}$, where Λ is the narrow-band integrated intensity. For the three isothermal cases, the results from the SNB model can be indeed treated as exact or the benchmark solution, assuming that the SNB gas transmissivity in isothermal and homogeneous media is exact. For the non-isothermal case, however, the SNB results can no longer be treated as exact, due to the use of the Curtis–Godson approximation, even though they are used as the reference solution in the evaluation of SNBCK results. Unless otherwise stated, results of the SNBCK method were calculated using the "7-point Gauss–Lobatto" and the three Gauss–Legendre quadratures.

Fig. 1 shows the narrow-band integrated intensities obtained for Column 1. Except for the SNBCK1 (hereafter SNBCKn denotes the SNBCK method using the n-point Gauss quadrature) results, results of the SNBCK2, SNBCK4, and SNBCK7 are all in good agreement with the SNB results. It is not surprising to observe that the SNBCK1 results are in large error based on the performance of the grey-band model (an equivalent form of the SNBCK1), previously evaluated by Liu et al. [4]. However, it is interesting to notice that the SNBCK2 results are much better than the SNBCK1 results, Fig. 1(a) and (b), with only one additional quadrature point used in the calculation. Except at spectral regions where the narrow-band integrated intensities are very low (around 2500, 4300, 6000, and beyond 7500 cm^{-1}), the relative errors of the SNBCK2 results are less than 6%. The SNBCK4 and the SNBCK7 results are very accurate compared to the SNB results with less than 3% error in almost the entire spectral region, Fig. 1(c), except in spectral regions around 4300 cm^{-1} and beyond 7500 cm^{-1}, where the mixture is almost non-radiating. The 4-point Gauss–Legendre quadrature performs almost equally well as the "7-point Gauss–Lobatto" quadrature with significantly less computing effort.

SNBCK calculations of narrow-band integrated intensities in Column 1 were also performed using the 4-point and 5-point Gauss–Lobatto quadratures. The errors and relative errors of these two quadratures are compared with those of the other three quadratures in Fig. 2. Except in spectral regions where the mixture strongly absorbs and emits, results of the SNBCK4 (Lobatto) and SNBCK5 (Lobatto) are even worse than the SNBCK2 results. The 2-point Gauss–Lobatto quadrature was also used for Column 1 calculation and the results (not shown) were found to be even much worse than those of the 1-point Gauss–Legendre quadrature. It is surprising to observe that the Gauss–Lobatto quadratures yield much worse results than the Gauss–Legendre ones in the SNBCK calculations. Therefore, the two Gauss–Lobatto quadratures were not included in the following evaluation.

Narrow-band intensities calculated for Column 2 are compared in Fig. 3. Although results of the SNBCK1 method are not shown, its performance is similar to that observed in Fig. 1. Again, narrow-band intensities calculated using the SNBCKn methods ($n > 1$) are in good agreement with those obtained using the SNB model, Fig. 3(a). The relative errors of the SNBCK methods for this shorter column, Fig. 3(c), are generally greater than those for the longer column displayed in Fig. 1(c). This is attributed to the increased quadrature errors in optically-thin media pointed out by Riv-

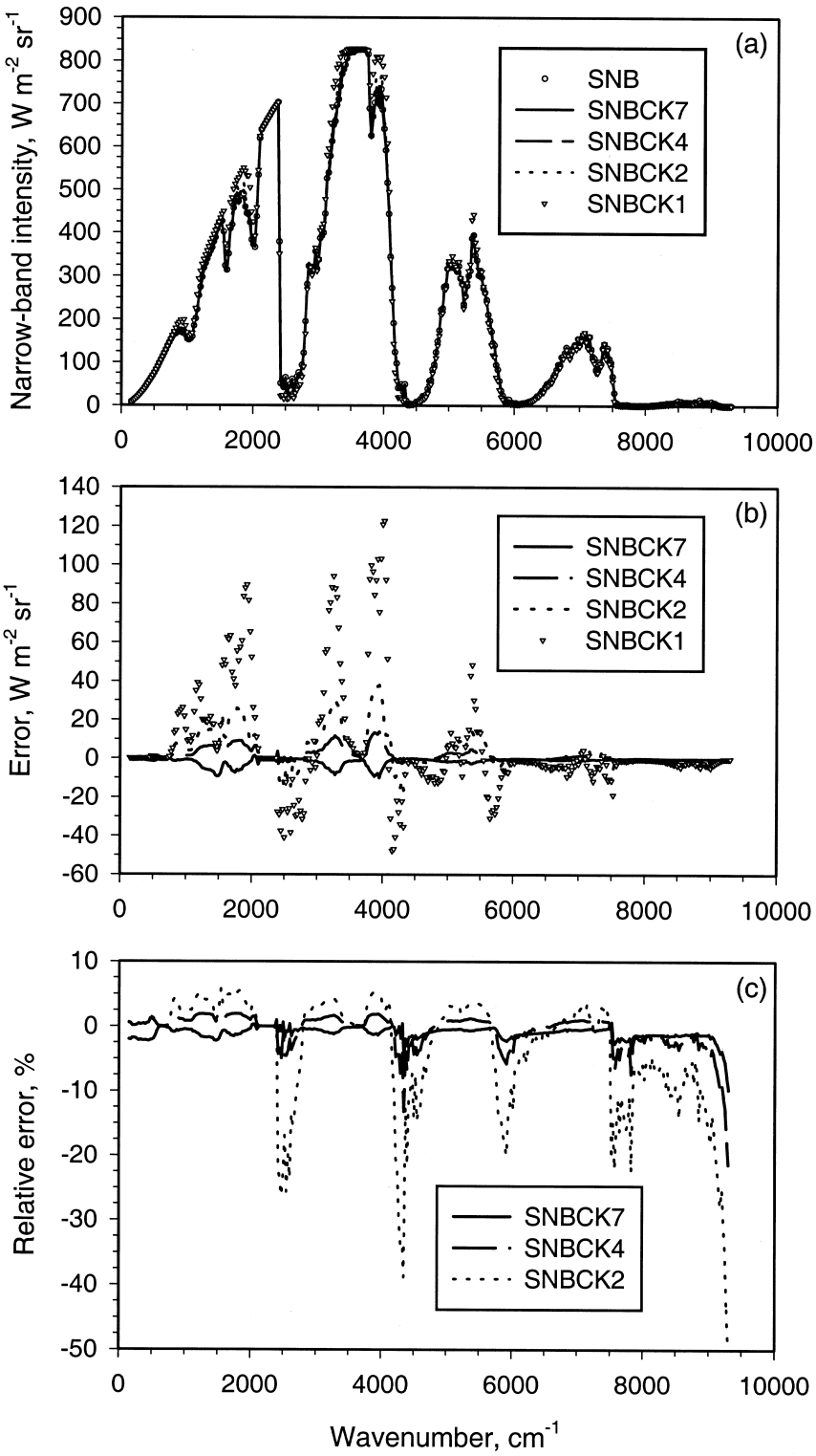

Fig. 1. Comparison of narrow-band integrated intensities, error, and relative error of the SNBCK method using four quadratures for Column 1.

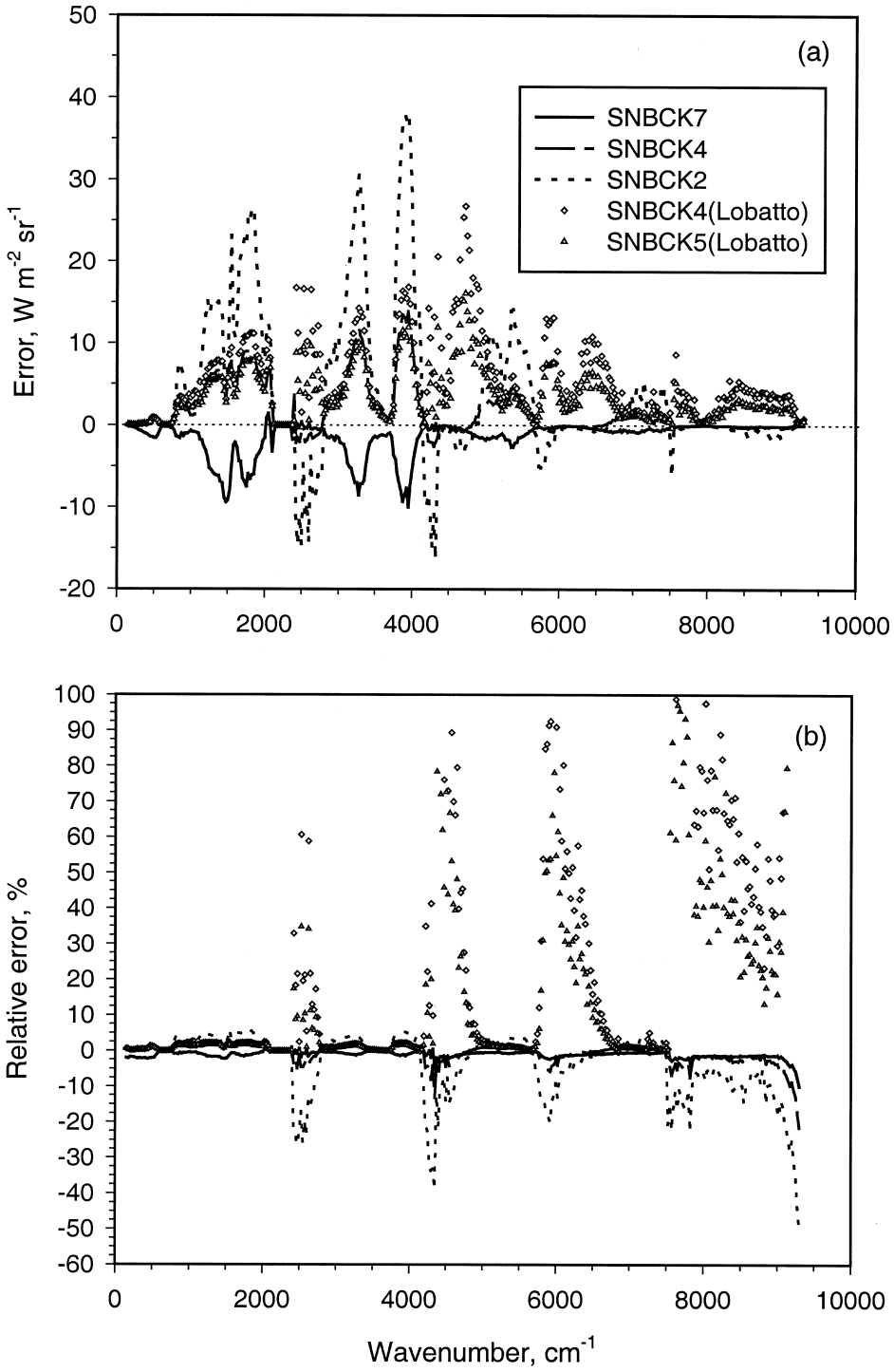

Fig. 2. Comparison of errors and relative errors of the SNBCK method using the 4-point, the 5-point Gauss–Lobatto, the "7-point Gauss–Lobatto", and the 4-point and the 2-point Gauss–Legendre quadratures for Column 1.

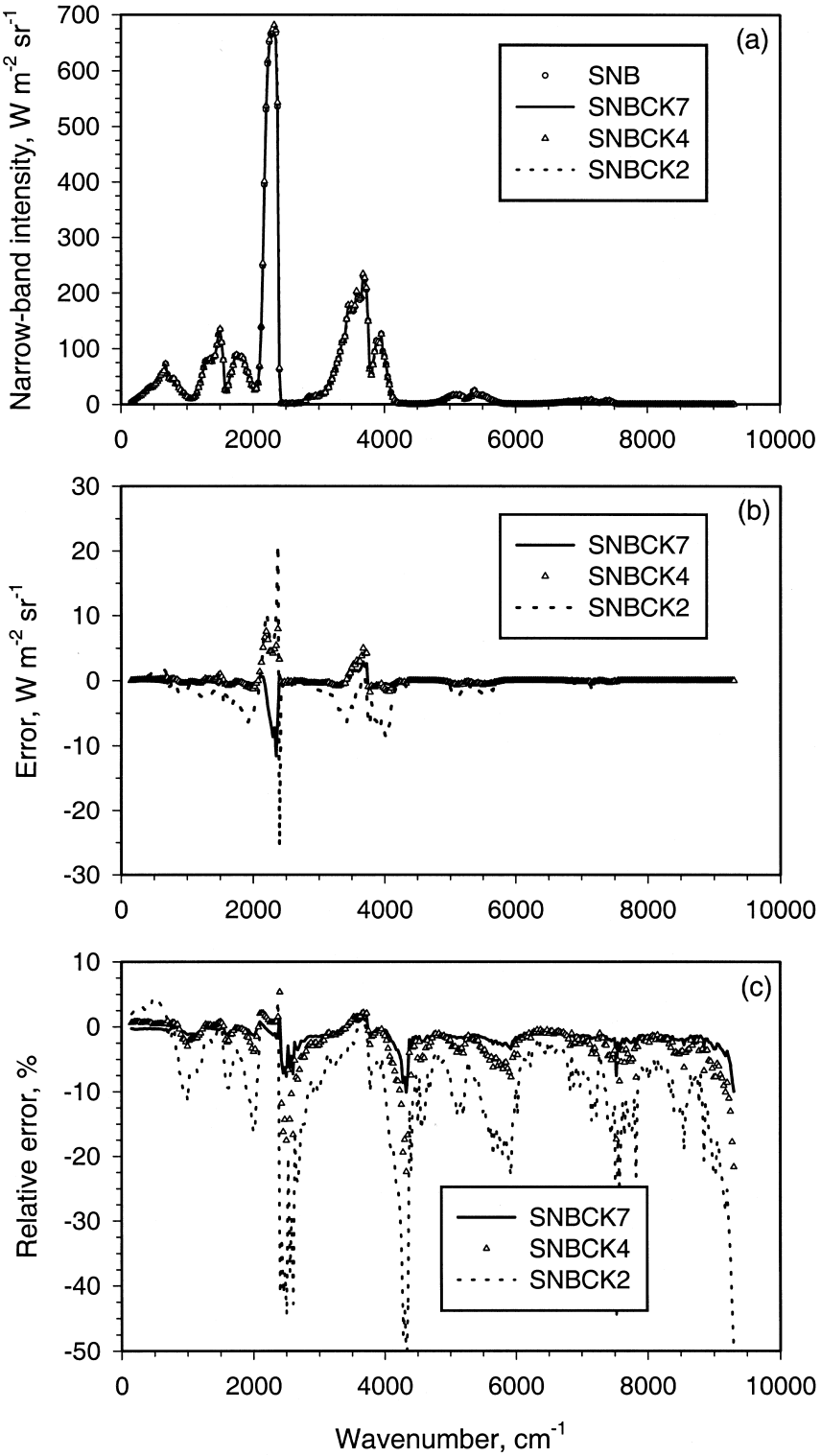

Fig. 3. Comparison of narrow-band integrated intensities, error, and relative error of the SNBCK method using four quadratures for Column 2.

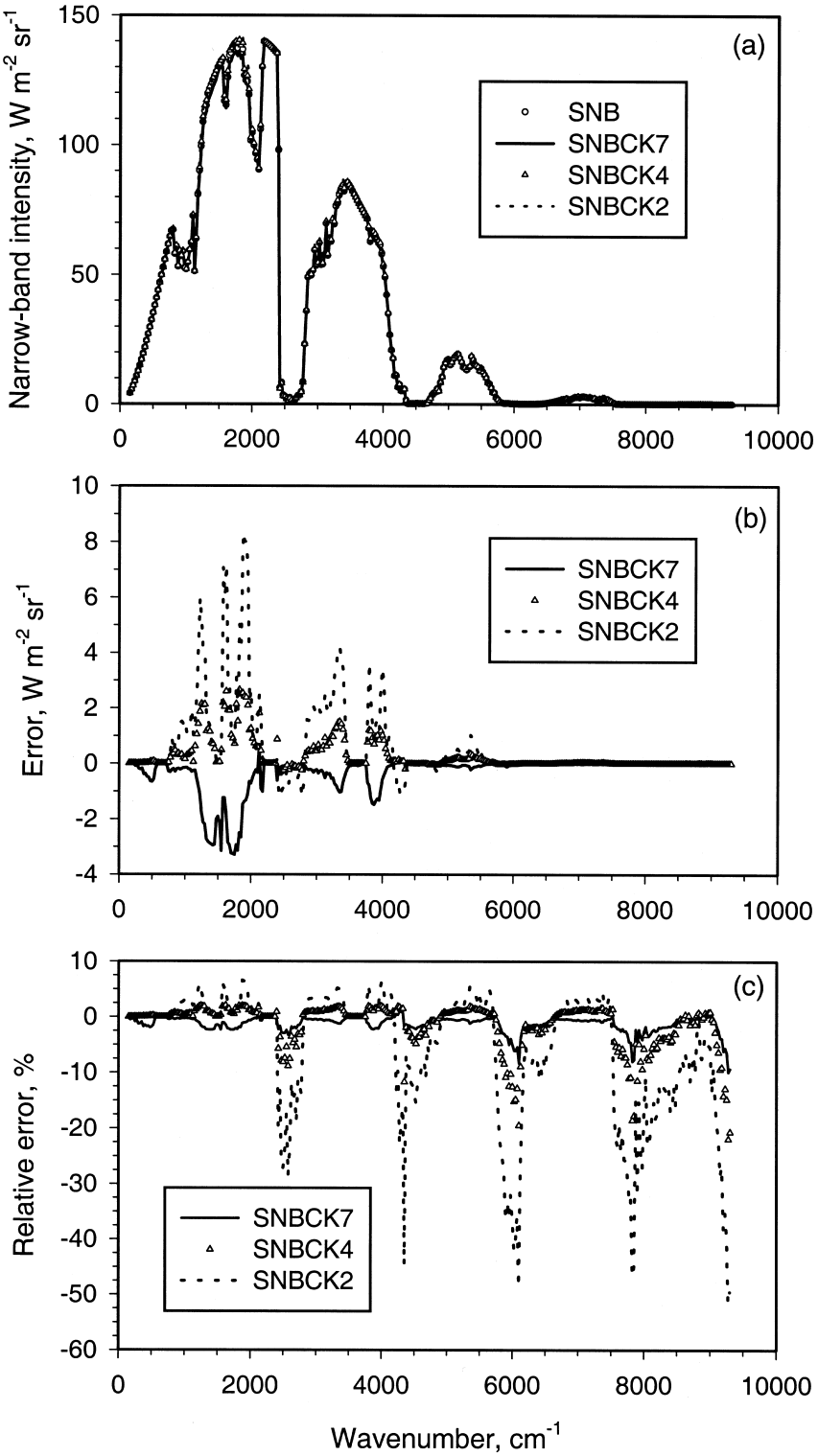

Fig. 4. Comparison of narrow-band integrated intensities, error, and relative error of the SNBCK method using four quadratures for Column 3.

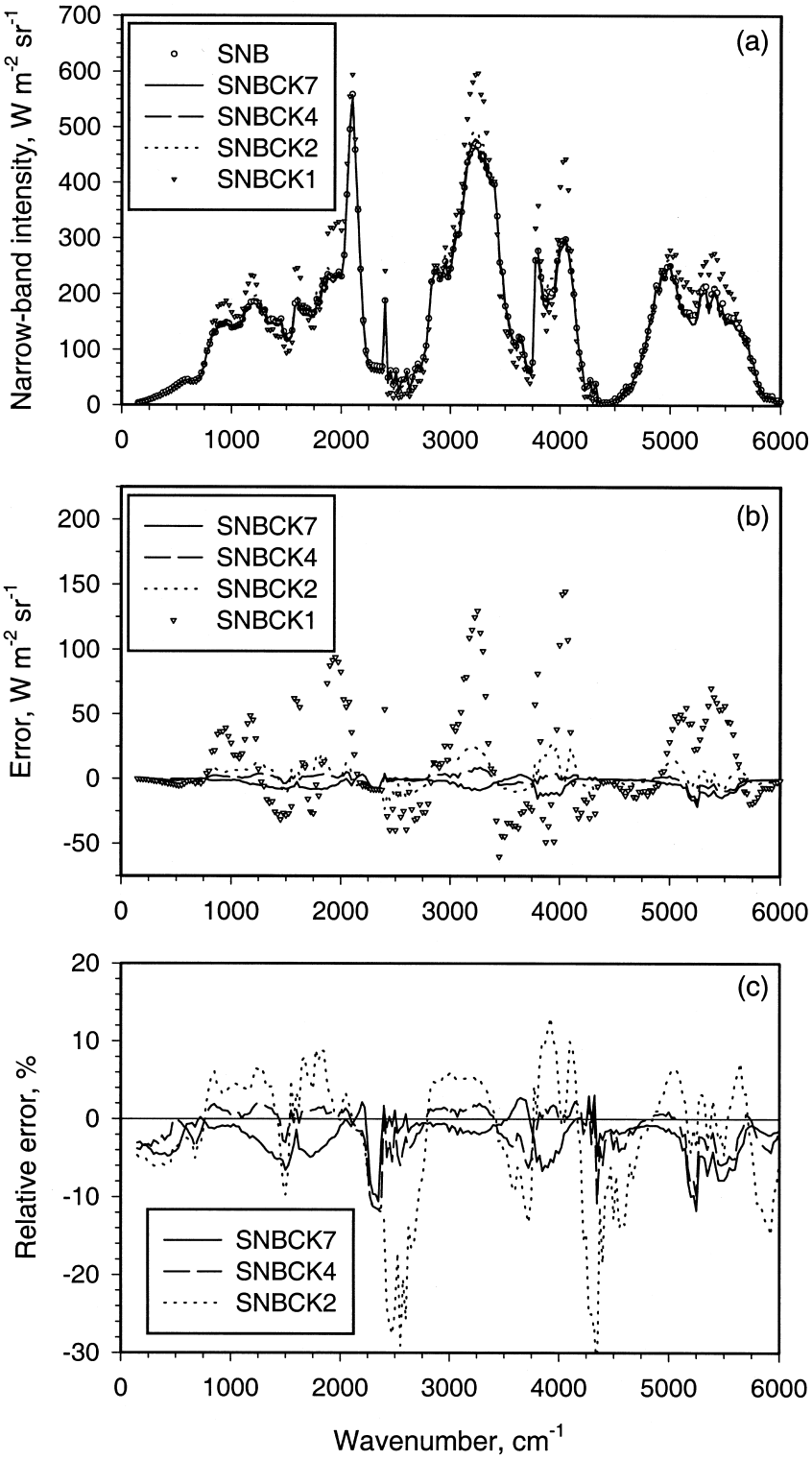

Fig. 5. Comparison of narrow-band integrated intensities, error, and relative error of the SNBCK method using four quadratures for Column 4.

ière et al. [6]. The relative errors of SNBCK4 and SNBCK7 results are still within a few percent at most of the spectral regions, while the errors of SNBCK2 results are generally within 20%, except at some narrow spectral regions.

Narrow-band integrated intensities for Column 3 are shown in Fig. 4. Good agreement is found between the SNBCK and the SNB results, Fig. 4(a). The relative errors of the SNBCK methods are again quite small and at similar levels to those of Column 1 shown in Fig. 1(c) at spectral regions where radiation intensities are relatively high.

For the non-isothermal case, narrow-band intensities between 150 and 6000 cm^{-1} are compared in Fig. 5. In this case, results of the SNB model contain errors through the Curtis–Godson approximation [11]. On the other hand, extra errors are introduced into the results of the SNBCK method through the scaling approximation [5,6] on top of the quadrature errors. Results of the 1-point SNBCK method are erroneous. A similar behaviour of the grey-band approximation (an alternative formulation of the 1-point SNBCK method) has been previously observed by Liu et al. [4]. In general, the SNBCKn ($n > 1$) results are in good agreement with the SNB results. The SNBCK4 and SNBCK7 results deviate from the SNB ones by less than 10%, while the errors of the SNBCK2 method are within 30% compared to the SNB results.

3.2. Spectrally integrated quantities in one-dimensional parallel-plates geometry

Real-gas radiation (spectrally integrated quantities) calculations in a one-dimensional parallel-plates enclosure were performed for four cases. In all the four cases, the wall surfaces are assumed to be black and the medium is at a uniform pressure of 1 atm. In the first case, the medium bounded by the two parallel plates is pure water vapour at a uniform temperature of 1000 K. The two bounding walls are cold (at 0 K). Two separation distances, $L = 0.1$ and 1 m, are considered in this case. The input parameters of the second case are the same as the first one, except that the medium now is a mixture of N_2 and H_2O with a parabolic H_2O concentration profile given by $f_{H_2O} = 4(1 - x/L)x/L$, and the separation distance is $L = 1$ m. In the third case, the medium is again pure H_2O with a boundary layer type temperature distribution [19]. The left wall is hot at $T_1 = 1500$ K and the right wall is cold at $T_2 = 300$ K. The separation distance is $L = 0.2$ m. These three test cases provide good testbeds to evaluate separately the effects of pathlength and gas temperature and concentration distributions on the results, and have been previously chosen as test cases by Kim et al. [19] and Liu et al. [7] using different solution methods and/or radiative property models. The fourth case considered has the same temperature distribution as the third case. However, the medium is now a mixture of 10% CO_2, 20% H_2O, and 70% N_2 (mole basis), instead of pure water vapour, and the separation distance is 0.5 m. This case was chosen to demonstrate the effect of the correlated treatment of overlapping bands on the computing time on the SNBCK method. Characteristics of the four test cases are summarised in Table 5. All the calculations were conducted using a 20 uniform grid and the T_4 quadrature.

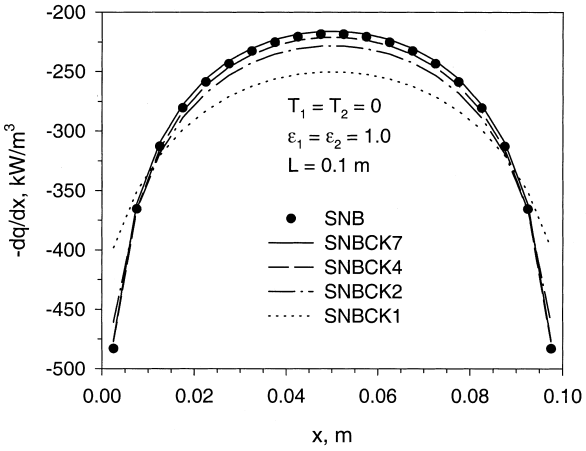

Fig. 6. Distributions of the calculated radiative source term in parallel-plates geometry for Case 1: $L = 0.1$ m.

Radiative source term distributions for Case 1 are compared in Figs. 6 and 7 for $L = 0.1$ and 1 m, respectively. For the small separation distance case, Fig. 6, the SNBCK1 results are in 16% error, while the errors of the SNBCK2 results are in only 4%.

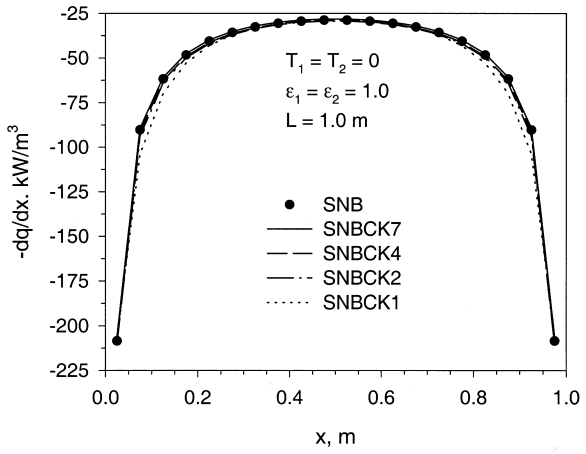

Fig. 7. Distributions of the calculated radiative source term in parallel-plates geometry for Case 1: $L = 1$ m.

Table 5
Computational conditions of the four test cases in the parallel-plates enclosure

Case	Species concentration profile	Temperature profile	L (m)
1	Pure water vapour	Uniform at 1000 K	0.1 and 1
2	Parabolic H_2O profile	Uniform at 1000 K	1
3	Pure water vapour	Boundary layer type	0.2
4	Homogeneous CO_2 + H_2O	Boundary layer type	0.5

Results of the SNB model, the SNBCK7, and SNBCK4 methods are in very good agreement. For the large separation distance case, Fig. 7, the SNB, SNBCK7, SNBCK4, and SNBCK2 results are almost identical. Even the SNBCK1 method yields quite accurate source term distribution. Results shown in Figs. 6 and 7 indicate that the accuracy of the SNBCK method deteriorates as the separation distance decreases. This behaviour of the SNBCK method has been observed from the narrow-band intensities along a line-of-sight, as shown in Figs. 1 and 3, where errors of the SNBCK results increase with decreasing the path-length.

Fig. 8 shows the source term distributions for Case 2. The SNB, SNBCK7 and SNBCK4 results are again in very good agreement. The SNBCK2 results are also quite accurate with less than 5% errors, except very close to the walls, where the errors are about 14%. Note that the mole fraction of H_2O is very low near the walls in this case. The SNBCK1 results are qualitatively correct but in serious error quantitatively.

The calculated radiative source term distribution for Case 3 are compared in Fig. 9. Except the 1-point SNBCK method, results of the other four methods are in very good agreement.

Radiative source term distributions calculated using the SNB model and the four SNBCK methods for Case 4 are shown in Fig. 10. Similar to what was found in Fig. 9, the 1-point SNBCK method yields inaccurate results and the results of the other four methods are in very good agreement with each other.

The CPU times of the SNBCK method using different quadratures for radiation transfer in H_2O (Cases 1–3) and CO_2–H_2O mixture (Case 4) are compared in Fig. 11. As can be expected, the CPU time increases linearly with the number of quadrature points for radiation transfer calculations in H_2O (Cases 1–3). For calculations in the CO_2–H_2O mixture (Case 4), the CPU time of the SNBCK method increases rapidly with the number of quadrature points due to the existence of 96 overlapping bands. The portion of extra CPU time spent on the treatment of overlapping bands increases quadratically with the number of the quadrature points. For example, the CPU time of the 7-point SNBCK calculation in the CO_2–H_2O mixture is 2.4 times of that in pure H_2O, while this ratio drops to 1.8, 1.3 and 1 when $N = 4$, 2, and 1, respectively.

Results of the heat flux density at the left wall are summarised in Table 6. All the SNBCK results are in good agreement with the SNB results for gas radiation in one-dimensional parallel-plates geometry under conditions investigated.

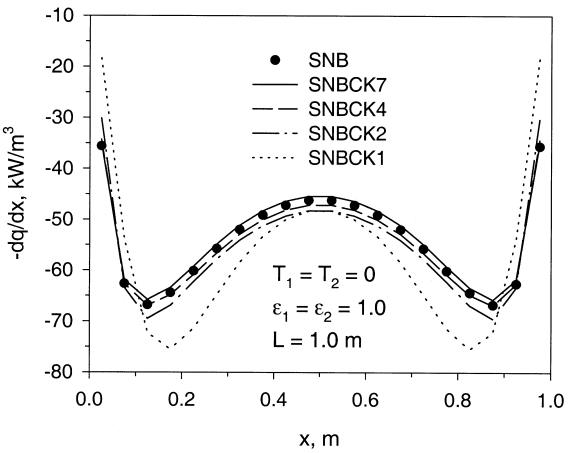

Fig. 8. Distributions of the calculated radiative source term in parallel-plates geometry for Case 2.

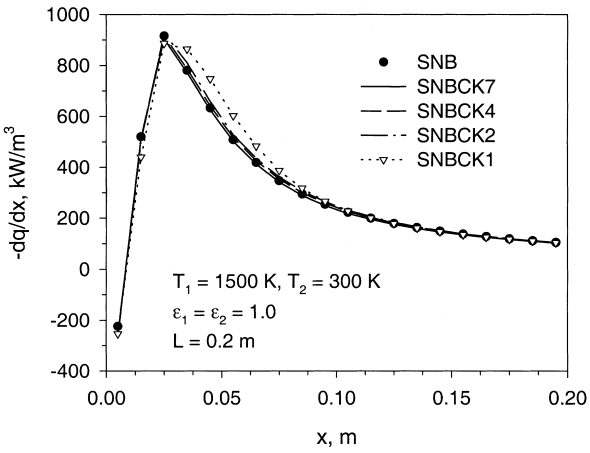

Fig. 9. Distributions of the calculated radiative source term in parallel-plates geometry for Case 3.

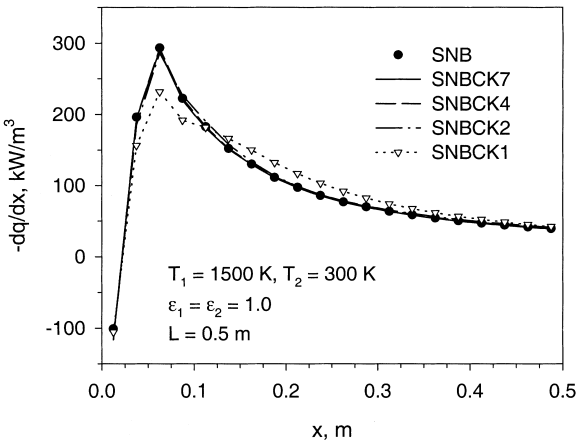

Fig. 10. Distributions of the calculated radiative source term in parallel-plates geometry for Case 4.

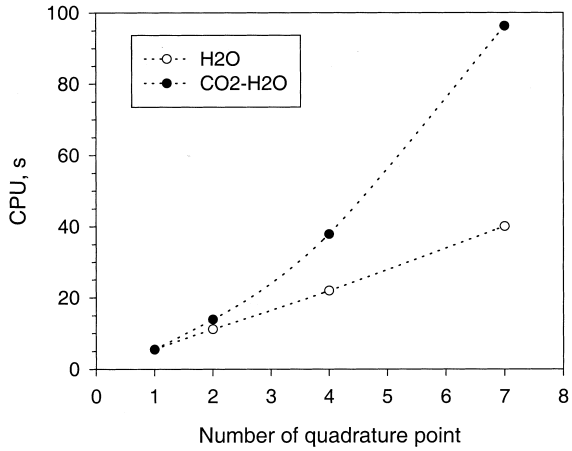

Fig. 11. Dependence of the CPU time of the SNBCK method on the number of quadrature points for calculations of radiative transfer in parallel-plates geometry.

3.3. Spectrally integrated quantities in a three-dimensional rectangular enclosure

The dimension of the enclosure is 2 m $\times$2 m $\times$ 4 m. All the surrounding walls are black and cold at 300 K. The pressure of the gas mixture in the enclosure is kept at 1 atm. The gas is a mixture of 10% CO_2, 20% H_2O and 70% N_2. The gas temperature is non-uniform but symmetrical about the centreline of the enclosure and is specified in terms of $T = (T_c - T_e)f(r/R) + T_e$. In this equation, T_c is the gas temperature along the centreline of the enclosure, T_e is the exit temperature at $z = 4$ m. Inside the circular region of the cross-section of the enclosure, the variation of gas temperature is defined by $f(r/R) = 1 - 3(r/R)^2 + 2(r/R)^3$, where r is the distance from the enclosure centreline and R is the radius of the circular region ($R = 1$ m). The gas temperature outside the circular region is assumed to be uniform and at the value of the exit temperature. The centreline temperature is assumed to increase linearly from 400 K at the inlet ($z = 0$) to 1800 K at $z = 0.375$ m, then decreases linearly to 800 K at the exit.

The RTE associated with the SNBCK method was solved using DOM. The spatial discretisation was achieved using the positive scheme and the T_4 quadrature set was used for angular discretisation, which contains 128 directions in three-dimensions. The enclosure was divided into 17 $\times$ 17 $\times$ 24 control volumes. A uniform grid was placed in the x- and y-directions and a non-uniform grid was used in the z-direction. For this test problem, numerical results of the wall heat flux and the volumetric source term was presented by Liu [20] using the SNB model alongwith a ray-tracing algorithm, and was used in the present evaluation as the reference solution.

Distributions of wall heat flux along the length of the enclosure at (2 m, 1 m, z) calculated using the SNBCK method and the four quadratures are compared in Fig. 12. Fig. 13 shows the volumetric source term distributions along the centreline of the enclosure, (1 m, 1 m, z). Results of the SNB model obtained by Liu [20] are also plotted as a reference. Although results of the SNBCK7 method are about 3% higher than those of the SNB model around the peak heat flux, Fig. 12, and about 4% lower around the minimum source term, Fig. 13, the discrepancies cannot be wholly attributed to the difference between the SNB model and the SNBCK7 method in this comparison, since two different solvers were used. The discrepancies between the results of the SNB model and the

Table 6
Comparison of predicted net heat fluxes at the left wall (kW/m^2)

Test case	SNB	SNBCK7	SNBCK4	SNBCK2	SNBCK1
Case 1, L = 0.1 m	−14.2	−14.0	−14.3	−14.5	−14.7
Case 1, L = 1 m	−30.3	−30.0	−30.6	−31.2	−31.7
Case 2	−27.0	−26.6	−27.2	−27.7	−28.3
Case 3	271.5	271.3	271.3	271.5	272.4

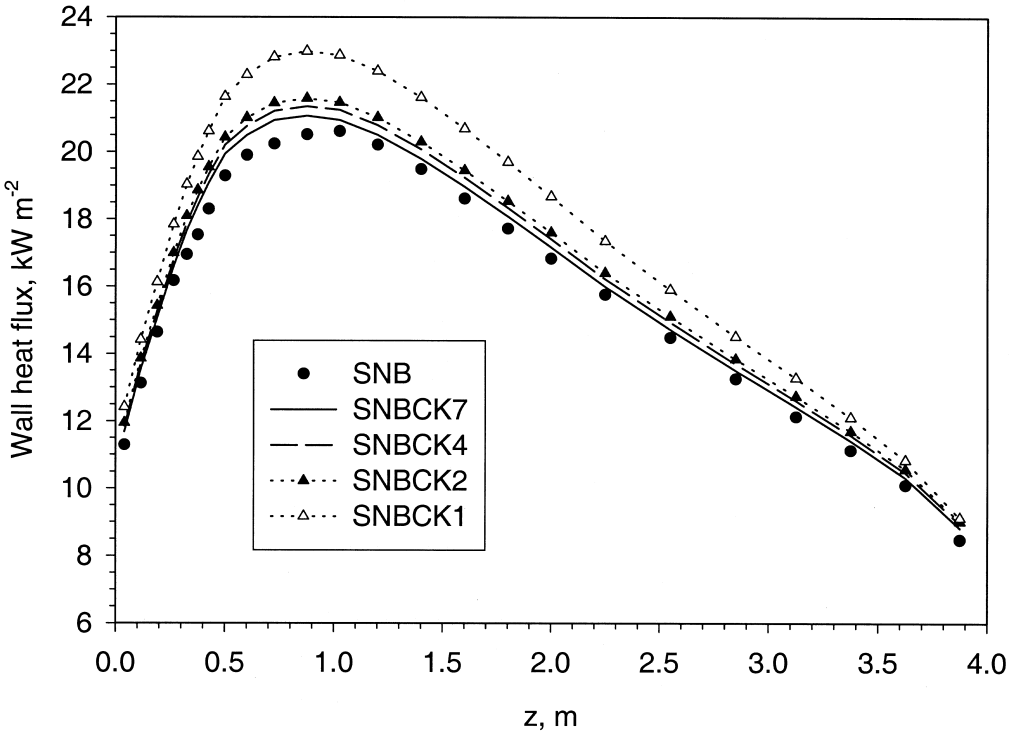

Fig. 12. Distributions of wall heat flux along z-direction at (2 m, 1 m, z) in the three-dimensional rectangular enclosure.

SNBCKn method can be attributed to the following three factors. First, some quadrature errors exist in the results of the SNBCK method as shown in Figs. 1, 3 and 4. Secondly, further approximations are introduced in both, the SNB model (Curtis–Godson approximation) and the SNBCK method (scaling approximation) for application to non-isothermal media. A quantitative assessment of these two approximations is beyond the scope of the present study. Thirdly, a ray-tracing algorithm was used to solve the RTE of the SNB model, while DOM was used in the SNBCK method. It is well known that the numerical results of DOM using conventional spatial differencing schemes (positive scheme is one of them) are relatively inaccurate in multidimensions [21]. On the other hand, a ray-tracing method offers better numerical accuracy for intensity calculations along a line-of-sight, albeit time-consuming to execute in three-dimensions, since the transfer equation is solved along a line-of-sight which is one-dimensional. However, in general, it requires a relatively large angular quadrature set to suppress errors due to ray effects. Therefore, the numerical inaccuracy of DOM is also responsible for the discrepancy between the results of the SNB model and the SNBCKn method. Despite these numerical and physical uncertainties, the discrepancies between the SNB model and the SNBCK7 method are quite small.

Compared to the wall heat fluxes of the SNBCK7 method, errors of the 4-point, 2-point and 1-point SNBCK methods are, respectively, 1.5, 2.5, and 9% around the peak heat flux shown in Fig. 12. For the source term distribution along the centreline of the enclosure, Fig. 13, results of the 7-point, 4-point, and 2-point SNBCK methods are almost identical. Errors of the 1-point SNBCK method are about 5.5% at the minimum value compared to the SNBCK7 results.

The CPU times the SNBCK calculations using the four quadratures are compared in Table 7. The CPU times of the 7-point SNBCK calculation is about 6.8 times of the 2-point SNBCK calculation and 2.6 times of the 4-point SNBCK calculation.

Table 7
CPU times the SNBCK calculations in the three-dimensional rectangular enclosure

N	CPU (s)
1	1298
2	3680
4	9777
7	25,020

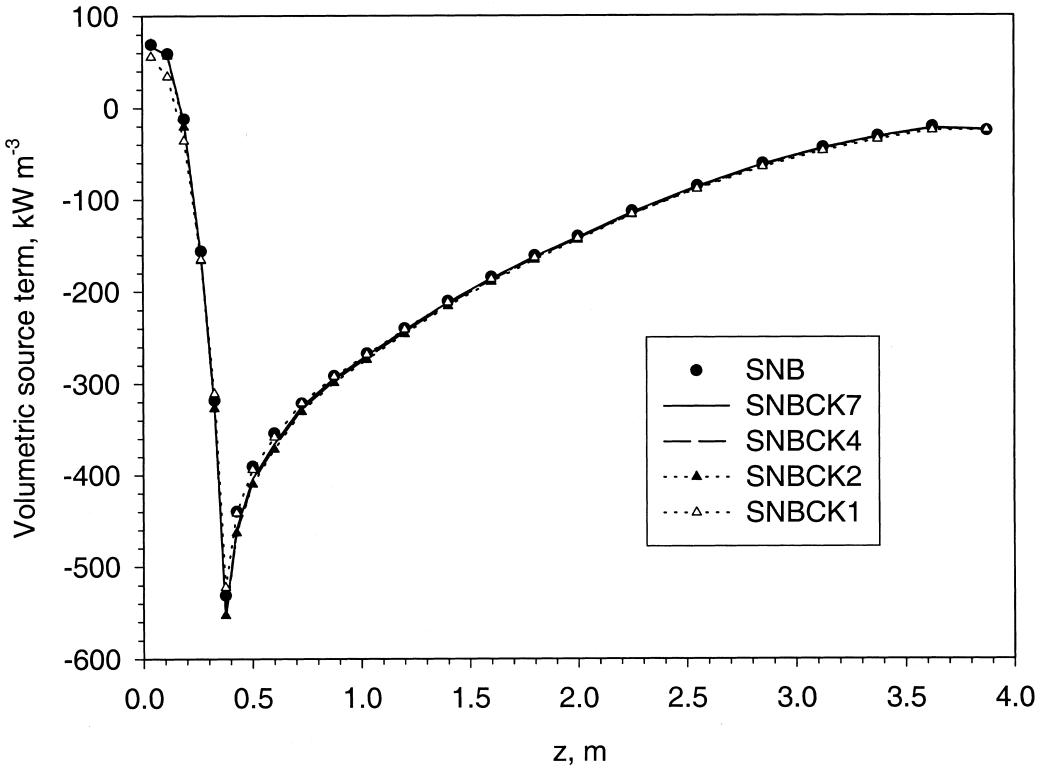

Fig. 13. Distributions of the radiative source term along the centreline of the three-dimensional rectangular enclosure.

4. Conclusions

Effects of quadrature on the accuracy and efficiency of the SNBCK method for real-gas radiation calculations have been investigated for both narrow-band intensities along a line-of-sight and spectrally integrated quantities in one-dimensional parallel-plates enclosures and in a three-dimensional rectangular enclosure containing CO_2–H_2O mixtures. The following conclusions are reached based on the numerical results of this study:

1. The SNBCK method is in general more accurate at bands where the mixture strongly absorbs and emits, and less accurate at bands where the mixture weakly absorbs and emits.
2. Results of the SNBCK method using the "7-point Gauss–Lobatto" quadrature are in very good agreement with the SNB model results. For narrow-band intensities calculations, the discrepancies between these two models are less than 5% at most of the spectral regions for isothermal problems, and within 10% for non-isothermal problems.
3. Use of the 4-point Gauss–Legendre quadrature in the SNBCK method in general yields similar accuracy to the "7-point Gauss–Lobatto" quadrature, while providing significant CPU time savings.
4. Use of Gauss–Lobatto quadratures yields poor results in SNBCK calculations and therefore, they are not recommended.
5. The 2-point Gauss–Legendre quadrature also yields reasonably good accuracy at most of the spectral regions for narrow-band intensities and good accuracy for spectrally integrated quantities, with even greater CPU time savings.
6. The 1-point Gauss–Legendre quadrature yields erroneous results especially for narrow-band intensities along a line-of-sight.
7. The 2-point Gauss–Legendre quadrature is recommended for spectrally integrated quantities calculations for multidimensional problems, based on its accuracy and efficiency.

References

[1] J.S. T'ien, H. Bedir, Radiative extinction of diffusion flames — a review, paper presented at the First Asia–Pacific Conference on Combustion, Osaka, Japan, 1997.
[2] M. Abid, M.S. Wu, J.B. Liu, P.D. Ronney, M. Ueki,

K. Maruta, H. Kobayashi, T. Niioka, Experimental and numerical study of flame ball IR and UV emissions, Combustion and Flame 116 (1999) 348–359.

[3] M.D. Smooke, C.S. McEnally, L.D. Pfefferle, R.J. Hall, M.B. Colket, Computational and experimental study of soot formation in a coflow, laminar diffusion flame, Combustion and Flame 117 (1999) 117–139.

[4] F. Liu, Ö.L. Gülder, G.J. Smallwood, Three-dimensional non-grey gas radiative transfer analysis using the statistical narrow-band model, Rev. Gén. Therm 37 (1998) 759–768.

[5] R.M. Goody, Y.L. Yung, Atmospheric Radiation, 2nd ed., Oxford University Press, UK, Oxford, 1989.

[6] Ph. Rivière, A. Soufiani, J. Taine, Correlated-*k* and fictious gas methods for H_2O near 2.7 μm, J. Quant. Spectrosc. Radiat. Transfer 48 (1992) 187–203.

[7] F. Liu, Ö.L. Gülder, G.J. Smallwood, Y. Ju, Non-grey gas radiative transfer analyses using the statistical narrow-band model, Int. J. Heat Mass Transfer 41 (1998) 2227–2236.

[8] V. Goutière, A. Charette, F. Liu, An assessment of real gas modelling in 2D enclosures, J. Quant. Spectro. Radiat. Transfer 64 (2000) 299–326.

[9] L. Pierrot, A. Soufiani, J. Taine, Accuracy of narrow-band and global models for radiative transfer in H_2O, CO_2, and H_2O–CO_2 mixtures at high temperature, J. Quant. Spectrosc. Radiat. Transfer 62 (1999) 523–548.

[10] S.S. Yang, T.-H. Song, An improved WSGGM-based narrow band model for CO_2 4.3 μm band, Int. J. Therm. Sci 38 (1999) 228–238.

[11] A. Soufiani, J. Taine, High temperature gas radiative property parameters of statistical narrow-band model for H_2O, CO_2 and CO, and correlated-*k* model for H_2O and CO_2, Int. J. Heat Mass Transfer 40 (1997) 987–991.

[12] A. Soufiani, Private communication, October, 1999.

[13] A.A. Lacis, V. Oinas, A description of the correlated-*k* distribution method for modeling nongray gaseous absorption, thermal emission, and multiple scattering in vertically inhomogeneous atmospheres, J. Geophysical Research 96 (1991) 9027–9063.

[14] F. Liu, G.J. Smallwood, Ö.L. Gülder, Application of the statistical narrow-band correlated-*k* method to non-grey gas radiation in CO_2–H_2O mixtures: approximate treatments of overlapping bands, submitted to J. Quant. Spectro. Radiat. Transfer (1999).

[15] R. Goody, R. West, L. Chen, D. Crisp, The correlated-*k* method for radiation calculations in nonhomogeneous atmospheres, J. Quant. Spectrosc. Radiat. Transfer 42 (1989) 539–550.

[16] P.Y.C. Lee, K.G.T. Hollands, G.D. Raithby, Reordering the absorption coefficient within the wide band for predicting gaseous radiant exchange, J. Heat Transfer 118 (1996) 384–400.

[17] K.C. Tang, M.Q. Brewster, Analysis of molecular gas radiation: real gas property effects, in: B.F. Armaly (Ed.), ASME Proceedings of the 7th AIAA/ASME Joint Thermophysics and Heat Transfer Conference, vol. 1, 1998, pp. 32–32.

[18] D.B. Ludwig, W. Malkmus, J.E. Reardon, J.A.L. Thomson, Handbook of Infrared Radiation from Combustion Gases, NASA SP3080 (1973).

[19] T.K. Kim, J.A. Menart, H.S. Lee, Nongray radiative gas analysis using the S–N discrete ordinates method, J. Heat Transfer 113 (1991) 946–952.

[20] F. Liu, Numerical solutions of three-dimensional non-grey gas radiative transfer using the statistical narrow-band model, J. Heat Transfer 121 (1999) 200–203.

[21] F. Liu, H.A. Becker, A. Pollard, Spatial differencing schemes of the discrete ordinates method, Numerical Heat Transfer. Part B 30 (1996) 23–43.